Mathematical Biosciences and Engineering

http://www.aimspress.com/journal/mbe

MBE, 20(2): 2131–2156.
DOI: 10.3934/mbe.2023099
Received: 29 August 2022
Revised: 30 September 2022
Accepted: 18 October 2022
Published: 15 November 2022

Research article

Robust adaptive neural network integrated fault-tolerant control for underactuated surface vessels with finite-time convergence and event-triggered inputs

Xiangfei Meng[1], Guichen Zhang[1,*] and Qiang Zhang[2,*]

[1] Merchant Marine College, Shanghai Maritime University, Shanghai 201306, China
[2] School of Navigation and Shipping, Shandong Jiaotong University, Weihai 264200, China

* **Correspondence:** Email: gczhang@shmtu.edu.cn, zq20060054@163.com.

Abstract: In this paper, we study the trajectory tracking control of underactuated surface vessels(USVs) subject to actuator faults, uncertain dynamics, unknown environmental disturbances, and communication resource constraints. Considering that the actuator is prone to bad faults, the uncertainties formed by the combination of fault factors, dynamic uncertainties and external disturbances are compensated by a single online updated adaptive parameter. In the compensation process, we combine the robust neural-damping technology with the minimum learning parameters (MLPs), which improves the compensation accuracy and reduces the computational complexity of the system. To further improve the steady-state performance and transient response of the system, finite-time control (FTC) theory is introduced into the design of the control scheme. At the same time, we adopt the event-triggered control (ETC) technology, which reduces the action frequency of the controller and effectively saves the remote communication resources of the system. The effectiveness of the proposed control scheme is verified by simulation. Simulation results show that the control scheme has high tracking accuracy and strong anti-interference ability. In addition, it can effectively compensate for the adverse influence of fault factors on the actuator, and save the remote communication resources of the system.

Keywords: fault-tolerant control; single parameter; finite-time control; event-triggered inputs; underactuated surface vessels

1. Introduction

With the continuous development of the marine economy, intelligent unmanned surface vessels have received special attention. To further improve the degree of automation of USVs, many studies focus on improving the tracking performance of the vessel control system [1–3]. Trajectory tracking

control is a very typical application scenario, which is often used to verify the effectiveness of control schemes [4–6]. And in actual engineering, many engineering tasks are unavoidable to avoid making the vessels track the predetermined trajectory, such as oil exploration, submarine cable laying, etc. The tracking performance of the vessel is usually limited by the following factors:

1) Internal uncertain dynamics and external unmeasurable unknown environmental disturbances lead to the failure to obtain accurate model information in the control scheme design.

2) For USVs performing missions in extreme environments, frequent actuator actions, as well as the physical limitations of propulsion and steering devices, lead to actuator failures, which seriously affect the tracking performance of the system.

The USVs trajectory tracking system has typical non-holonomic constraint characteristics. Under the constraints physical, constraints of the actuator, the design of the control scheme needs to consider more factors. (Pettersen et al. [7] and Do [8]) respectively used differential homeomorphism and additional control methods to solve the underactuation problem. The method in [7] converted the mathematical model of USVs into two chained subsystems through changes and stabilized the system errors indirectly by designing control laws. In [8], by constructing a virtual transverse drive vector, the virtual control variables of the original propulsion system were decomposed through a coordinate transformation to achieve the purpose of applying part of the longitudinal drive to the transverse direction. However, both were control schemes designed based on accurate models. In other words, prior knowledge of the model must be obtained in advance. (Zhang et al. [9]) carried out the state transition for the system and considered the uncertain terms in the model. However, this method imposes a norm limit on transverse and longitudinal errors in the design process, and the implicit assumption is that the heading error must be less than 0.5 PI. In [10], new kinematic and dynamic equations were obtained by using the definition of hands, and the control scheme was designed by combining the vector method. However, both the underactuated transformation and the NNs algorithm used by the system may bring huge computational load to the system.

In practice, the vessel's control system cannot execute arbitrary control instructions. This is caused by the saturation limit of the actuator. The steady state of the control system is challenged by the non-smooth property of the saturation function. In numerous studies, there are two main types of saturation. One method is to use the strong robustness of the control system to force the system error to stabilize. The other is to adopt the active compensation method. For example, auxiliary system design, smooth function approximation, and other methods. In [11], the smooth property of the Gaussian error function was used to replace the non-linearity of the saturation function. However, the control scheme is designed on the basis of a fully actuated system. In addition, (Zheng [12]) used a hyperbolic tangent function to replace the nonlinearity caused by the non-smooth saturation function, but this method increases the complexity of the control scheme design.

In the actual ocean voyage, due to the limitation of modeling technology and the unmeasurable ocean environment, the tracking system cannot obtain the model dynamic parameters and the prior information of unknown external disturbances in advance. Therefore, the vessel will inevitably be affected by internal and external uncertainties. In view of the dynamic uncertainty of the USVs, it is a very popular way to use intelligent control algorithms such as fuzzy or NNs to reconstruct the vessel. (Zhou et al. [13] and Kong et al. [14]) designed the control scheme combined with the adaptive theory without obtaining the prior information of the model. (Huang et al. [15]) combined with a disturbance observer to compensate for the unmeasurable disturbances and further improved the tracking accuracy

on the basis of [13] and [14]. Although the control effect of an intelligent algorithm is very considerable, we cannot ignore the huge load faced by the system. In other words, these burdens are unbearable in real control systems. In order to solve this problem, (Zhang et al. [16]) converted the uncertainty of the system into a single parameter form by combining the minimum learning parameter, which effectively reduced the computational pressure of the system. However, the norm calculation method tended to be conservative obviously, that is to say, we must inevitably sacrifice part of the tracking accuracy. To solve this problem, a nonlinear function was introduced in [17] to filter the error through nonlinear feedback.

For a USVs control system in normal operation, the stability of the system highly depends on the normal operation of the actuator. However, when the USVs are operating, harsh sea conditions are inevitable and the equipment is often subjected to seawater erosion. These adverse conditions may become potential failure factors for the actuator. Therefore, developing a fault-tolerant control scheme will undoubtedly improve the reliability of the vessel control system. In dynamic systems, adaptive control is a common method compensating for the fault factors acting on the actuator. (Cai et al. [18]) and (Tang et al. [19]) designed fault-tolerant control schemes for strictly nonlinear systems and multi-input multi-output systems, respectively. (Wang er al. [20] and Zheng et al. [21]) had applied the submethod in a marine surface vessel control system. However, reference [21] only considered bias faults.

References [18–21] are all based on time-triggered control strategies, which will lead to broadband congestion, aggravation of actuator wear, and other problems. On the contrary, an event-triggered policy transfers control commands to the actuator only if the trigger condition is violated. Avoid the huge communication burden brought about by the vessel control system in periodic control mode. At the same time, the actuator does not have to repeatedly receive control commands, so as to effectively reduce the failure rate of the equipment. Control schemes based on event-triggered control design had been widely used in trajectory-tracking control [22–24]. (Xing et al. [25]) designed a novel fault-tolerant control scheme based on an event trigger mechanism. Subsequently, (Zhang et al. [26] and Zhu et al. [27]) had done similar research on course-keeping control and trajectory-tracking control, respectively. All of them effectively compensate for the uncertain effect of fault factors in the system. However, these control schemes only achieved convergence when the system time tends to infinity. FTC can effectively improve the transient response steady-state performance of the system, which cannot be ignored. Many authors have proved this conclusion [28–32]. If the idea of FTC is incorporated into the design of a fault-tolerant control scheme, the tracking accuracy of the system will be further guaranteed. Inspired by the above references, this paper designs a novel fault-tolerant control scheme. The specific contributions of this paper are as follows:

1) In this study, we consider both internal and external uncertain dynamics. Reconstructing the dynamic uncertainty with RBFNNs combined with MLPs reduces the computational load of the system. It is worth noting that the proposed control scheme does not require real-time updates of the neural network weights.

2) Without prior knowledge of the model, the effects of input saturation limits and actuator faults are considered. The relative threshold event trigger strategy is adopted to reduce the frequent update of control commands and reduce actuator wear. The unknown factors including bias fault factors and partial failure fault factors, as well as other unknown factors of the system are dynamically transformed into a single-parameter linearized form, which is compensated by an adaptive parameter updated on-

line.

2. Problem formulation and preliminaries

In general, the 3-DOF mathematical model of USV tracking control can be expressed in the following form [22, 33]:

$$\begin{cases} \dot{x} = u\cos(\psi) - v\sin(\psi) \\ \dot{y} = u\sin(\psi) + v\cos(\psi) \\ \dot{\psi} = r \end{cases} \tag{2.1}$$

$$\begin{cases} \dot{u} = \frac{1}{m_u}\left[\ \tau_u^f\ + f_u(u,v,r) + d_u\right] \\ \dot{v} = \frac{1}{m_v}\left[f_v(u,v,r) + d_v\right] \\ \dot{r} = \frac{1}{m_r}\left[\ \tau_r^f\ + f_r(u,v,r) + d_r\right] \end{cases} \tag{2.2}$$

$$\begin{cases} f_u(u,v,r) = (m_v vr - Y_{\dot{r}} r^2 + X_u u + X_{u|u|}|u|u) \\ f_v(u,v,r) = (Y_v v + Y_{|v|v}|v|v + Y_{|r|v}|r|v + Y_r r - m_u ur + Y_{|v|r}|v|r + Y_{|r|r}|r|r) \\ f_r(u,v,r) = \left[(m_u - m_v)uv + Y_{\dot{r}} ur + N_v v + N_r r + N_{|r|v}|r|v + N_{|v|v}|v|v + N_{|v|r}|v|r + N_{|r|r}|r|r\right] \end{cases} \tag{2.3}$$

where x, y, ψ represent the position and heading angle of the USV in the geodetic coordinate system, respectively. u, v, r represent the surge velocity, sway velocity and yaw velocity, respectively. $f_u(u,v,r)$, $f_v(u,v,r)$, $f_r(u,v,r)$ are the non-linear dynamics, respectively. m_i, $(i = u, v, r)$ are the inertial mass. d_u, d_v, d_r represent the unmeasurable unknown disturbances, respectively. τ_u^f, τ_r^f are the surge control force and the yaw control force due to actuator failure, respectively. In this work, we focus on the Loss-of-effectiveness (LOE) and bias fault, the specific form is as follows:

$$\tau_i^f = \varrho_i \tau_i + \sigma_i \tag{2.4}$$

if $\varrho_i = 1$, $\sigma_i = 0$, it means that the unmanned ship system is fault-free. If $0 < \varrho_i < 1$, $\sigma_i = 0$, it means that the actuator is suffering from a LOE fault. If $\varrho_i = 1$, $0 < \sigma_i < 1$, it means that the actuator is suffering from a bias fault.

In engineering practice, ship actuators inevitably suffer from physical limitations, which make the control inputs τ_u^f, τ_r^f affected by input saturation, which are described as follows [27]:

$$\tau_i = \begin{cases} \mathrm{sgn}(\tau_i)\,\tau_{i,\max}, & \text{if } \left|\tau_{i,c}\right| > \tau_{i,\max} \\ \tau_{i,c}, & \text{if } \left|\tau_{i,c}\right| < \tau_{i,\max} \end{cases} \tag{2.5}$$

In view of the design of control law, the following assumptions are made and relevant definitions and theorems are introduced:

Assumption 1. $f_i(u,v,r)$, $(i = u, v, r)$ are unknown. The external disturbance d_i, $(i = u, v, r)$ unknown and bounded. So there are unknown positive constants σ_u, σ_v, σ_r such that d_u, d_v, d_r satisfy $|d_u| \le \sigma_u$, $|d_u| \le \sigma_v$, $|d_u| \le \sigma_r$.

Definition 1. [34, 35] Nonlinear control systems are described as follows system (2.6)

$$\dot{x} = f(x), x(0) = x_o, x \in \Omega_0 \subset R^n \tag{2.6}$$

where $x \in R^n$ is the state variable of the system, Ω_0 is a spherical domain containing the origin, and $f(x)$ is a continuous function. For any initial condition x_0, if there is a constant $\Im > 0$ and a regulating

time function $0 < T(x_o) < \infty$ such that $\|x(t)\| \leq \Im$, $t \geq T(x_0)$, then the system (2.6) can be said to be semi-globally practical finite-time stable.

Lemma 1. [36] For the nonlinear system (2.6), assuming that there is a positive definite Lyapunov function $V(x)$: $\Omega_0 \to R$ and any scalar $a > 0$, $b > 0$ and $0 < \kappa < 1$ such that the inequality $\dot{V}(x) + aV(x) + bV^{\kappa}(x) \leq 0$ holds, the system (2.6) is stable in finite time, and its adjustment time satisfies:

$$T \leq \frac{1}{a(1-t)} \ln \frac{aV^{1-\kappa}(x_0) + b}{b} \tag{2.7}$$

where $V(x_0)$ is the initial value of $V(x)$.

Lemma 2. [37, 38] For any given continuous smooth function defined on the compact set $\Omega \subset R^n$

$$h(x) = W^{*T} s(x) + \varepsilon, \forall x \in \Omega \tag{2.8}$$

where ε is the approximation error, and for all $x \in \Omega$, here is a vector $\varepsilon^* > 0$, and $|\varepsilon| \leq \varepsilon^*$ is satisfied. $s(x)$ is the NN basis function, which is represented by a Gaussian function, as follows:

$$s(x) = \exp\left[\frac{-(\mathbf{X} - \mathbf{c}_i)^T (\mathbf{X} - \mathbf{c}_i)}{\omega_i^2}\right] \tag{2.9}$$

where $\mathbf{c}_i$ is the center vector, and ω_i is the width of the Gaussian function. W^* is the weight vector under ideal conditions. Usually the ideal neural network weight vector is an unknown vector and needs to be estimated. It can be understood that $|\varepsilon|$ can minimize ω on $x \in \Omega \subset R^n$, that is

$$W^* := \arg\min_{W \in R^l} \left\{ \sup_{x \in \Omega} \left| h(x) - W^{\mathrm{T}} S(x) \right| \right\} \tag{2.10}$$

Assumption 2. In the compact set $\Omega_x \subset R^n$, the weight W^* of the RBFNNs used to approximate the unknown vector is bounded, that is, $\|W^*\| \leq W_M$, where W_M is a positive constant.

Lemma 3. [39] For any constant $\varsigma > 0$ and any scalar $\rho \in R$, inequality (2.11) holds

$$0 \leq |\rho| - \frac{\rho^2}{\sqrt{\rho^2 + \varsigma^2}} < \varsigma \tag{2.11}$$

Lemma 4. [40] For any $a > 0$ and $x \in R$, the following relation is satisfied.

$$0 < |x| - x \tanh\left(\frac{x}{a}\right) \leq 0.2785a \tag{2.12}$$

3. Control design and stability analysis

First, define the tracking error as follows

$$z_e = \begin{bmatrix} x_e \\ y_e \end{bmatrix} = \begin{bmatrix} x - x^* \\ y - y^* \end{bmatrix} \tag{3.1}$$

where x^*, y^*, are the reference position of the USV.

Taking the derivation of Eq (3.1), one can get

$$\dot{z}_e = ug_u(\psi) + vg_v(\psi) - \begin{pmatrix} \dot{x}^* \\ \dot{y}^* \end{pmatrix} \tag{3.2}$$

where $g_u(\psi) = \begin{bmatrix} \cos(\psi) \\ \sin(\psi) \end{bmatrix}$, $g_v(\psi) = \begin{bmatrix} -\sin(\psi) \\ \cos(\psi) \end{bmatrix}$.

The virtual control law is designed to stabilize the error z_e as follows:

$$\alpha = \begin{pmatrix} \alpha_x \\ \alpha_y \end{pmatrix} = u^* g_u(\psi^*) = -k_{11}z_e - \frac{k_{12}z_e}{\sqrt{\|z_e\|^2 + \varsigma_z{}^2}} - vg_v(\psi) + \begin{pmatrix} \dot{x}^* \\ \dot{y}^* \end{pmatrix} \tag{3.3}$$

where k_{11}, k_{12} are positive definite parameters.

It is not difficult to obtain the relationship in Eq (3.4) by further calculating Eq (3.3)

$$\begin{cases} u^* = \|\alpha\| \\ \psi^* = \arctan\left(\alpha_y, \alpha_x\right) \end{cases} \tag{3.4}$$

where u^* is the reference surge velocity, ψ^* is the reference heading angle.

The heading angle error is defined as follows:

$$\psi_e = \psi - \psi^* \tag{3.5}$$

Taking the derivation of Eq (3.5), we can get

$$\dot{\psi}_e = r - \dot{\psi}^* \tag{3.6}$$

To stabilize the error ψ_e a virtual control variables of the following form is designed:

$$r^* = -k_{31}\psi_e - \frac{k_{32}\psi_e}{\sqrt{|\psi_e|^2 + \varsigma_\psi{}^2}} + \dot{\psi}^* \tag{3.7}$$

where k_{31} and k_{32} are positive definite parameters.

Filter u^* and r^* by using dynamic stability control (DSC) technology

$$\begin{cases} \eta_u\dot{\beta}_u + \beta_u = u^* \\ \eta_r\dot{\beta}_r + \beta_r = r^* \end{cases} \tag{3.8}$$

where the dynamic surface error $e_{f,u} = \beta_u - u_d$, $e_{f,r} = \beta_r - r_d$.

According to Eqs (3.2)–(3.8), it can be obtained

$$\begin{cases} \dot{z}_e = -k_{11}z_e - \frac{k_{12}z_e}{\sqrt{\|z_e\|^2 + \varsigma_z{}^2}} + \Delta_e \\ \dot{\psi}_e = -k_{31}\psi_e - \frac{k_{32}\psi_e}{\sqrt{|\psi_e|^2 + \varsigma_\psi{}^2}} + r_e \end{cases} \tag{3.9}$$

where $\Delta_e = ug_u(\psi) - u^* g_u(\psi^*)$.

The velocity error variable is defined as follows

$$\begin{cases} u_e = u - \beta_u \\ r_e = r - \beta_r \end{cases} \tag{3.10}$$

Taking the derivation of Eq (3.10), one can get

$$\begin{cases} \dot{u}_e = \frac{1}{m_u}\left(\tau_u^f \ + f_u(u,v,r) + d_u \right) - \dot{u}^* \\ r_e = \frac{1}{m_r}\left(\tau_r^f \ + f_r(u,v,r) + d_r \right) - \dot{r}^* \end{cases} \tag{3.11}$$

Since $f_u(u,v,r)$ and $f_r(u,v,r)$ are unknown, they cannot be used in the design of the controller. Therefore, the RBFNNs are used to approximate the unknown nonlinear functions.

$$\begin{cases} f_u(u,v,r) = {W_u}^T \sigma_u(\eta) + \varepsilon_u \\ f_r(u,v,r) = {W_r}^T \sigma_r(\eta) + \varepsilon_r \end{cases} \tag{3.12}$$

where W_u and W_r are the neural network weights. $\sigma_u(\eta)$ and $\sigma_r(\eta)$ are the NN functions. ε_u and ε_r are approximation errors. Substituting Eq (3.12) into Eq (3.11), one can get

$$\begin{cases} \dot{u}_e = \frac{1}{m_u}\left(\varrho_u \tau_u + \sigma_u + {W_u}^T \sigma_u(\eta) + \varepsilon_u + d_u \right) - \dot{\beta}_u \\ r_e = \frac{1}{m_r}\left(\varrho_r \tau_r + \sigma_r + {W_r}^T \sigma_r(\eta) + \varepsilon_r + d_r \right) - \dot{\beta}_r \end{cases} \tag{3.13}$$

Next, by combining the idea of the relative threshold event triggering mechanism, the following dynamic event triggering mechanism is designed [25]

$$\begin{cases} \tau_u(t) \ = \omega_u(t_k), \forall t \in [t_k, t_{k+1}) \\ t_{k+1} = \inf\{ t \in R \,||e_u(t)| \geq \eta_{12} |\tau_u(t)| + \eta_{11} \} \end{cases} \tag{3.14}$$

$$\begin{cases} \tau_r(t) \ = \omega_r(t_k), \forall t \in [t_k, t_{k+1}) \\ t_{k+1} = \inf\{ t \in R \,||e_r(t)| \geq \eta_{22} |\tau_r(t)| + \eta_{21} \} \end{cases} \tag{3.15}$$

where $e_u(t)$, $e_r(t)$ are the measurement errors, and η_{11}, η_{12}, η_{21}, η_{22} re the positive definite design parameters. t_k is the update time of the controller. During the time interval $t \in [t_k, t_{k+1}]$, the control input $\omega_u(t_k)$ and $\omega_r(t_k)$ remains unchanged. When the moment switches to t_{k+1}, a new control command will be sent to the actuator.

Under this event triggering mechanism, $|\omega_u(t) - \tau_u(t)| \leq \eta_{12}|\tau_u(t)| + \eta_{11}$ and $|\omega_r(t) - \tau_r(t)| \leq \eta_{22}|\tau_r(t)| + \eta_{21}$ are satisfied within any time. From this, when $\left|\lambda_{u,1}(t)\right| \leq 1$, $\left|\lambda_{u,2}(t)\right| \leq 1$, $\left|\lambda_{r,1}(t)\right| \leq 1$, $\left|\lambda_{r,2}(t)\right| \leq 1$, it is not difficult to draw the following relationship

$$\begin{cases} \omega_u(t) = \left[1 + \lambda_{u,1}(t)\eta_{12}\right] \ \tau_u(t) \ + \lambda_{u,2}(t)\eta_{11} \\ \omega_r(t) = \left[1 + \lambda_{r,1}(t)\eta_{22}\right] \ \tau_r(t) \ + \lambda_{r,2}(t)\eta_{21} \end{cases} \tag{3.16}$$

Further, the following relationship can be obtained

$$\begin{cases} \tau_u(t) \ = \frac{\omega_u(t)}{1+\lambda_{u,1}(t)\eta_{12}} - \frac{\lambda_{u,2}(t)\eta_{11}}{1+\lambda_{u,1}(t)\eta_{12}} \\ \tau_r(t) \ = \frac{\omega_r(t)}{1+\lambda_{r,1}(t)\eta_{22}} - \frac{\lambda_{r,2}(t)\eta_{21}}{1+\lambda_{r,1}(t)\eta_{22}} \end{cases} \tag{3.17}$$

According to Eqs (3.14)–(3.17), the velocity error becomes

$$\begin{cases} \dot{u}_e = \frac{1}{m_u}\left[\frac{\varrho_u \omega_u(t)}{1+\lambda_{u,1}(t)\eta_{12}} - \frac{\varrho_u \lambda_{u,2}(t)\eta_{11}}{1+\lambda_{u,1}(t)\eta_{12}} + \sigma_u + {W_u}^T \sigma_u(\eta) + \varepsilon_u + d_u \right] - \dot{\beta}_u \\ \dot{r}_e = \frac{1}{m_r}\left[\frac{\varrho_r \omega_r(t)}{1+\lambda_{r,1}(t)\eta_{22}} - \frac{\varrho_r \lambda_{r,2}(t)\eta_{21}}{1+\lambda_{r,1}(t)\eta_{22}} + \sigma_r + {W_r}^T \sigma_r(\eta) + \varepsilon_r + d_u \right] - \dot{\beta}_r \end{cases} \tag{3.18}$$

where $\frac{\varrho_u}{1+\lambda_{u,1}(t)\eta_{12}}$ and $\frac{\varrho_r}{1+\lambda_{r,1}(t)\eta_{22}}$ are nonlinear bounded functions with positive definite upper bound less than 1.

Combined with the design idea of the robust adaptive method of depth information, using the RBFNNs and the MLPs, we can further obtain

$$\begin{cases} \left\|W_u{}^T\sigma_u(\eta)+\varepsilon_u+d_u-m_u\dot{\beta}_u\right\| \le \left\|W_u{}^T\right\|\|\sigma_u(\eta)\| + \left|\varepsilon_u+d_u-m_u\dot{\beta}_u\right| = \wp_u\zeta_u(Z) \\ \left\|W_r{}^T\sigma_r(\eta)+\varepsilon_r+d_r-m_r\dot{\beta}_r\right\| \le \left\|W_r{}^T\right\|\|\sigma_r(\eta)\| + \left|\varepsilon_r+d_r-m_r\dot{\beta}_r\right| = \wp_r\zeta_r(Z) \end{cases} \tag{3.19}$$

where $\begin{cases} \wp_u = \max\left\{\left\|W_u{}^T\right\|, \left|\varepsilon_u+d_u-m_u\dot{\beta}_u\right|\right\} \\ \wp_r = \max\left\{\left\|W_r{}^T\right\|, \left|\varepsilon_r+d_r-m_r\dot{\beta}_r\right|\right\} \end{cases}$, $\begin{cases} \zeta_u(Z) = \|\sigma_u(\eta)\|+1 \\ \zeta_r(Z) = \|\sigma_r(\eta)\|+1 \end{cases}$. With the transformation, the adaptive learning parameters are significantly reduced.

To stabilize the influence of the fault factor on the system, the following variables is designed [25, 26]

$$\begin{cases} \Omega_u = \frac{1}{m_u}\left(\frac{\varrho_u\lambda_{u,2}(t)\eta_{11}}{1+\lambda_{u,1}(t)\eta_{12}} - \sigma_u + \wp_u\zeta_u(Z)\right) = \delta_u\varpi_u \\ \Omega_r = \frac{1}{m_r}\left(\frac{\varrho_u\lambda_{r,2}(t)\eta_{21}}{1+\lambda_{r,1}(t)\eta_{22}} - \sigma_r + \wp_r\zeta_r(Z)\right) = \delta_r\varpi_r \end{cases} \tag{3.20}$$

where $\delta_u = \frac{\varrho_u}{m_u\left(1+\lambda_{u,1}(t)\eta_{12}\right)}$, $\varpi_u = \frac{1+\lambda_{u,1}(t)\eta_{12}}{\varrho_u}\left(\frac{\varrho_u\lambda_{u,2}(t)\eta_{11}}{1+\lambda_{u,1}(t)\eta_{12}} - \sigma_u + \wp_u\zeta_u(Z)\right)$, $\delta_r = \frac{\varrho_r}{m_r\left(1+\lambda_{r,1}(t)\eta_{22}\right)}$, $\varpi_r = \frac{1+\lambda_{r,1}(t)\eta_{22}}{\varrho_r}\left(\frac{\varrho_r\lambda_{r,2}(t)\eta_{21}}{1+\lambda_{r,1}(t)\eta_{22}} - \sigma_r + \wp_r\zeta_r(Z)\right)$.

Through analysis, the dynamic error equation of the system becomes

$$\begin{cases} \dot{u}_e \le \delta_u\varpi_u + \frac{1}{m_u}\delta_u\omega_u(t) \\ \dot{r}_e \le \delta_r\varpi_r + \frac{1}{m_r}\delta_r\omega_r(t) \end{cases} \tag{3.21}$$

In view of this, the following control law is designed

$$\begin{cases} \omega_u(t) = m_u\left[-k_{21}u_e - \frac{k_{22}u_e}{\sqrt{|u_e|^2+\varsigma_u{}^2}} - \tanh\left(\frac{u_e}{\varepsilon_u}\right)\hat{\bar{\varpi}}_u\right] \\ \omega_r(t) = m_r\left[-k_{41}r_e - \frac{k_{42}r_e}{\sqrt{|r_e|^2+\varsigma_r{}^2}} - \tanh\left(\frac{r_e}{\varepsilon_r}\right)\hat{\bar{\varpi}}_r - \psi_e\right] \end{cases} \tag{3.22}$$

The adaptive law as follows

$$\begin{cases} \dot{\hat{\bar{\varpi}}}_u = c_1\left[\tanh\left(\frac{u_e}{\varepsilon_u}\right) - \iota_1\hat{\bar{\varpi}}_u\right] \\ \dot{\hat{\bar{\varpi}}}_r = c_2\left[\tanh\left(\frac{r_e}{\varepsilon_r}\right) - \iota_2\hat{\bar{\varpi}}_r\right] \end{cases} \tag{3.23}$$

Introduce the following Lyapunov function

$$V = \frac{1}{2}z_e{}^Tz_e + \frac{1}{2}\psi_e{}^2 + \frac{1}{2}u_e{}^2 + \frac{1}{2}r_e{}^2 + \frac{\delta_u}{2c_1}\tilde{\bar{\varpi}}_u{}^2 + \frac{\delta_r}{2c_2}\tilde{\bar{\varpi}}_r{}^2 \tag{3.24}$$

where $\tilde{\bar{\varpi}}_i = \bar{\varpi}_i - \hat{\bar{\varpi}}_i$, $i = u, r$.

Then, derivation of Eq (3.24) can be obtained

$$\dot{V} = z_e{}^T\dot{z}_e + \psi_e\dot{\psi}_e + u_e\dot{u}_e + r_e\dot{r}_e - \frac{\delta_u}{c_3}\tilde{\bar{\varpi}}_u\dot{\hat{\bar{\varpi}}}_u - \frac{\delta_r}{c_4}\tilde{\bar{\varpi}}_r\dot{\hat{\bar{\varpi}}}_r \tag{3.25}$$

According to Eqs (3.1)–(3.9), $|\beta_u - u^*| \le \gamma_u$, $|\beta_r - r^*| \le \gamma_r$ and Young's inequality, we can get

$$z_e{}^T \dot{z}_e + \psi_e \dot{\psi}_e = -z_e{}^T k_{11} z_e - \frac{z_e{}^T k_{12} z_e}{\sqrt{\|z_e\|^2 + \varsigma_z^2}} + z_e{}^T \Delta_e - k_{31} \psi_e{}^2 - \frac{k_{32} \psi_e{}^2}{\sqrt{|\psi_e|^2 + \varsigma_\psi^2}} + \psi_e r_e + \frac{\gamma_u + \gamma_r}{2} \tag{3.26}$$

In view of Eqs (3.10)–(3.23), and from Lemma 4, we can get

$$\begin{aligned} u_e \dot{u}_e - \frac{\delta_u}{c_3} \tilde{\bar{\varpi}}_u \dot{\hat{\bar{\varpi}}}_u \le & \delta_u u_e \left[-k_{21} r_e - \frac{k_{22} u_e}{\sqrt{|u_e|^2 + \varsigma_u{}^2}} + \varpi_u - \mathrm{Tanh}\left(\frac{u_e}{\varepsilon_u}\right) \hat{\bar{\varpi}}_u \right] \\ & - \delta_u \hat{\bar{\varpi}}_u \left[\mathrm{Tanh}\left(\frac{u_e}{\varepsilon_u}\right) u_e - \iota_1 \hat{\bar{\varpi}}_u \right] \\ \le & \delta_u \left(-k_{21} u_e{}^2 - \frac{k_{22} u_e{}^2}{\sqrt{|u_e|^2 + \varsigma_u{}^2}} + 0.2785 \varepsilon_u \bar{\varpi}_u - \frac{\iota_1}{2} \tilde{\bar{\varpi}}_u{}^2 + \frac{\iota_1}{2} \bar{\varpi}_u{}^2 \right) \end{aligned} \tag{3.27}$$

$$\begin{aligned} r_e \dot{r}_e - \frac{\delta_r}{c_4} \tilde{\bar{\varpi}}_r \dot{\hat{\bar{\varpi}}}_r \le & \delta_r r_e \left[-k_{41} r_e - \frac{k_{42} r_e}{\sqrt{|r_e|^2 + S_r^2}} - \psi_e + \varpi_r - \mathrm{Tanh}\left(\frac{r_e}{\varepsilon_r}\right) \hat{\bar{\varpi}}_r \right] \\ & - \delta_r \tilde{\bar{\varpi}}_r \left[\mathrm{Tanh}\left(\frac{r_e}{\varepsilon_r}\right) r_e - \iota_2 \hat{\bar{\varpi}}_r \right] \\ \le & \delta_r \left(-k_{41} r_e^2 - \frac{k_{42} r_e^2}{\sqrt{r_e^2 + \varsigma_r^2}} - r_e \psi_e + 0.2785 \varepsilon_r \bar{\varpi}_r - \frac{\iota_2}{2} \tilde{\bar{\varpi}}_r^2 + \frac{\iota_2}{2} \bar{\varpi}_r^2 \right) \end{aligned} \tag{3.28}$$

Substitute Eqs (3.26)–(3.28) into Eq (3.24), and according to $0 < \delta_i < 1$, $i = u, r$, we can get

$$\begin{aligned} \ddot{V} \le & - z_e{}^T \kappa_{11} z_e - \kappa_{12} \|z_e\| - \kappa_{11} \psi_e{}^2 - \kappa_{12} |\psi_e| \\ & - \kappa_{21} u_e^2 - \kappa_{22} |u_e| - \frac{\iota_1}{2} \delta_u \tilde{\bar{\varpi}}_u^2 + \frac{\iota_1}{2} \bar{\varpi}_u^2 + 0.2785 \varepsilon_u \bar{\varpi}_u \\ & - \kappa_{21} r_e^2 - \kappa_{22} |r_e| - \frac{\iota_2}{2} \delta_r \tilde{\bar{\varpi}}_r{}^2 + \frac{\iota_2}{2} \bar{\varpi}_r^2 + 0.2785 \varepsilon_r \bar{\varpi}_r \\ & + \frac{\gamma_u + \gamma_r}{2} + \frac{5}{2} \Delta_e{}^2 + \varsigma_{\max} (\kappa_{12} + \kappa_{22}) \end{aligned} \tag{3.29}$$

where $\kappa_{11} = \min\{(k_{11} - 0.1), k_{31}\}$, $\kappa_{12} = \min\{k_{12}, k_{32}\}$, $\kappa_{21} = \min\{\delta_u k_{21}, \delta_r k_{41}\}$, $\kappa_{22} = \min\{\delta_u k_{22}, \delta_r k_{42}\}$.

According to Young's inequality, we can get

$$\begin{cases} \frac{\iota_1}{4} \left| \tilde{\bar{\varpi}}_u \right| \le \frac{\iota_1}{4} \left| \tilde{\bar{\varpi}}_u \right|^2 + \frac{\iota_1}{16} \\ \frac{\iota_2}{4} \left| \tilde{\bar{\varpi}}_r \right| \le \frac{\iota_2}{4} \left| \tilde{\bar{\varpi}}_r \right|^2 + \frac{\iota_2}{16} \end{cases} \tag{3.30}$$

Substitute Eq (3.30) into Eq (3.29), and further obtain

$$\begin{aligned} \dot{V} \le & - z_e{}^T \kappa_{11} z_e - \kappa_{12} \|z_e\| - \kappa_{11} \psi_e{}^2 - \kappa_{12} \|\psi_e\| - \kappa_{21} u_e{}^2 - \kappa_{22} \|u_e\| - \kappa_{21} r_e{}^2 - \kappa_{22} \|r_e\| \\ & - \tfrac{\iota_1}{4} \delta_u \tilde{\bar{\varpi}}_u{}^2 - \tfrac{\iota_1}{4} \delta_u \left| \tilde{\bar{\varpi}}_u \right| + \tfrac{\iota_1}{2} \bar{\varpi}_u^2 - \tfrac{\iota_2}{4} \delta_r \tilde{\bar{\varpi}}_r{}^2 - \tfrac{\iota_2}{4} \delta_r \left| \tilde{\bar{\varpi}}_r \right| + \tfrac{\iota_2}{2} \bar{\varpi}_r^2 \\ & + 0.2785 (\varepsilon_u \bar{\varpi}_u + \varepsilon_r \bar{\varpi}_r) + \tfrac{5}{2} \Delta_e{}^2 + \tfrac{\iota_1 + \iota_2}{16} + \tfrac{\gamma_u + \gamma_r}{2} \\ \le & - \tfrac{\rho_1}{2} \left(z_e{}^T z_e + u_e{}^2 + \tfrac{\delta_u}{c_1} \tilde{\bar{\varpi}}_u{}^2 + \psi_e{}^2 + r_e{}^2 + \tfrac{\delta_r}{c_2} \tilde{\bar{\varpi}}_r{}^2 \right) \\ & - \rho_2 \left[\left(\tfrac{1}{2} z_e{}^T z_e \right)^{\frac{1}{2}} + \left(\tfrac{1}{2} u_e{}^2 \right)^{\frac{1}{2}} + \left(\tfrac{\delta_u}{2\bar{\varpi}_u} \tilde{\bar{\varpi}}_u{}^2 \right)^{\frac{1}{2}} + \left(\tfrac{1}{2} \psi_e{}^2 \right)^{\frac{1}{2}} + \left(\tfrac{1}{2} r_e{}^2 \right)^{\frac{1}{2}} + \left(\tfrac{\delta_r}{2\bar{\varpi}_r} \tilde{\bar{\varpi}}_r{}^2 \right)^{\frac{1}{2}} \right] + \Theta \\ \le & - \rho_1 V - \rho_2 V^{\frac{1}{2}} + \Theta \end{aligned} \tag{3.31}$$

where $\rho_1 = \min\left\{2\kappa_{11}, 2\kappa_{21}, \frac{\iota_1 c_1}{2}, \frac{\iota_2 c_2}{2}\right\}$, $\rho_2 = 2^{\frac{1}{2}} \min\left\{\kappa_{12}, \kappa_{22}, \frac{\iota_1 c_1}{4}, \frac{\iota_2 c_2}{4}\right\}$, $\Theta = \frac{\iota_3}{2}\bar{\varpi}_u^2 + \frac{\iota_4}{2}\bar{\varpi}_r^2 + \frac{\gamma_u+\gamma_r}{2} + 0.2785\left(\varepsilon_u\bar{\varpi}_u + \varepsilon_r\bar{\varpi}_r\right) + \frac{5}{2}{\Delta_e}^2 + \frac{\iota_1+\iota_2}{16}$.

According to Eq (3.31), one can get

$$\dot{V} \leq -\ell\rho_1 V - (1-\ell)\rho_1 V - \rho_2 V^{\frac{1}{2}} + \Theta \tag{3.32}$$

where $0 < \ell < 1$.

According to Eq (3.32), if $V > \frac{\Theta}{\ell\rho_1}$, one can get

$$\dot{V} \leq -(1-\ell)\rho_1 V - \rho_2 V^{\frac{1}{2}} \tag{3.33}$$

According to Lemma 1, it can be known that the system will stabilize to the region c in finite time, and the stabilization time is

$$T \leq \frac{4}{(1-\ell)\rho_1} \ln\left[\frac{(1-\ell)\rho_1 V^{1/2}(0) + \rho_2}{\rho_2}\right] \tag{3.34}$$

where $V(0)$ is the initial value of V.

According to the measurement error $e_u = \omega_u(t) - \tau_u(t)$, $e_r = \omega_r(t) - \tau_r(t)$, one can get

$$\begin{cases} \frac{d}{dt}|e_u| = \frac{d}{dt}(e_u * e_u)^{\frac{1}{2}} = sign(e_u)\dot{e}_u \leq |\dot{\omega}_u(t)| \\ \frac{d}{dt}|e_r| = \frac{d}{dt}(e_r * e_r)^{\frac{1}{2}} = sign(e_r)\dot{e}_r \leq |\dot{\omega}_r(t)| \end{cases} \tag{3.35}$$

Since all the variables that make up $\omega_u(t)$, $\omega_r(t)$ are globally bounded, $\omega_u(t)$, $\omega_r(t)$ are continuous. Therefore, there must be positive definite constants ζ_u, ζ_r, satisfying the conditions $|\dot{\omega}_u(t)| \leq \zeta_u$, $|\dot{\omega}_r(t)| \leq \zeta_r$.When $t = t_k$, there are $e_u(t_k) = 0$, $e_r(t_k) = 0$, $\lim\limits_{t\to t_{k+1}} e_u(t) = \eta_{12}|\tau_u(t)| + \eta_{11}$ and $\lim\limits_{t\to t_{k+1}} e_r(t) = \eta_{22}|\tau_r(t)| + \eta_{21}$. Therefore, there must be time intervals ${t_u}^*$ and ${t_r}^*$ satisfying ${t_u}^* \geq \frac{\eta_{12}|\tau_u(t)|-\eta_{11}}{\zeta_u}$, ${t_r}^* \geq \frac{\eta_{22}|\tau_r(t)|-\eta_{21}}{\zeta_r}$, which can avoid Zeno behavior.

4. Simulation

In this section, we select Cybership 2 model for simulation, and its parameters are detailed in [41]. In order to verify the effectiveness of the designed ETC trajectory tracking control scheme, the time-varying disturbance of Eq (4.1) is selected to simulate the external uncertain disturbance in the actual voyage, which is detailed as follows

$$\begin{cases} d_u = 11/12\left[1 + 0.35\sin(0.3t) + 0.15\cos(0.5t)\right] \\ d_v = 26/17.76\left[1 + 0.3\sin(0.4t) + 0.2\cos(0.1t)\right] \\ d_r = 950/636\left[1 + 0.3\sin(0.3t) + 0.1\cos(0.5t)\right] \end{cases} \tag{4.1}$$

In addition, the specific forms of LOE fault and bias fault are as follows

$$\begin{cases} \varrho_u = 0.6 + 0.4\exp(-0.2t) \\ \varrho_r = 0.8 + 0.2\exp(-0.1t) \end{cases} \tag{4.2}$$

$$\begin{cases} \sigma_u = 0.2 + 0.5\sin(0.1t) \\ \sigma_r = 0.2 + 0.6\cos(0.1t) \end{cases} \tag{4.3}$$

In order to quantitatively analyze the tracking performance of the control scheme designed in this paper, the integrated absolute error (IAE) and mean integrated absolute control (MIAC) of Eq (4.4) are used to evaluate the steady-state performance and energy consumption performance.

$$\begin{cases} \text{IAE} = \int_0^{t_f} |\upsilon_e|\, dt, \upsilon = x, y \\ \text{MIAC} = \frac{1}{t_f}\int_0^{t_f} |\omega_i(t)|\, dt, i = u.r \end{cases} \tag{4.4}$$

In this paper, two sets of simulation experiments are carried out under the circular reference trajectory and the trapezoidal reference trajectory.

4.1. Simulation experiment 1

The circular reference trajectory is as follows

$$\begin{cases} x^* = 25\sin(0.01\pi t) \\ y^* = 25 - 25\cos(0.01\pi t) \end{cases} \tag{4.5}$$

The controller parameters under the circular trajectory are shown in Table 1.

Table 1. Controller parameters.

Circular trajectory	$k_{11} = 0.2$	$k_{12} = 0.03$	$k_{21} = 0.8$	$k_{22} = 0.2$
	$k_{31} = 2.0$	$k_{32} = 0.3$	$k_{41} = 0.8$	$k_{42} = 0.3$
	$c_1 = 0.1$	$\iota_1 = 0.01$	$c_2 = 0.01$	$\iota_1 = 1$
	$\varsigma_z = 0.05$	$\varsigma_\psi = 0.05$	$\varsigma_u = 0.05$	$\varsigma_r = 0.05$
	$\eta_{11} = 0.05$	$\eta_{12} = 0.05$	$\eta_{21} = 0.05$	$\eta_{22} = 0.05$
	$\varepsilon_u = 0.05$	$\varepsilon_r = 0.05$		

Table 2. Performance index comparison of the schemes of ETC and FTC.

		ETC scheme	FTC scheme
IAE	$x - x^*$	6.6594	6.4818
	$y - y^*$	84.1017	85.1983
MIAC	τ_u	0.5945	0.5941
	τ_r	0.7903	0.6599

The data in Figures 1–10 and Table 2 show that the USVs system shows satisfactory tracking performance under the constraints of input saturation, actuator failure, communication congestion and other conditions. Under the two control schemes, the errors of the system are all within a reasonable range. First, under the constraints of actuator saturation, Figure 6 shows that the control inputs to the system are all within a reasonable range. According to the performance index data of MIAC in Table 2, the energy consumption of the ETC scheme is slightly higher than that of the continuous FTC scheme.

However, within the simulation time, the controller updates for the continuous control scheme both are 20,000 times, compared to 2636 and 574 times for the ETC scheme. On the contrary, the ECT control scheme in this paper effectively reduces the frequency of updating of the controller instructions. Figures 4 and 5 show the tracking error trend of the system with time, respectively, which are bounded under the two fault-tolerant control schemes. According to the performance index given by IAE in Table 2, the tracking accuracy of the continuous FT fault-tolerant control scheme is slightly better than that of the ETC control scheme. Figure 9 shows the time interval of event triggering, we can clearly see that the control instruction does not trigger infinite times in a very short period of time. Figure 7 and 8 show that both the NN weights and the estimates of the uncertain terms are bounded.

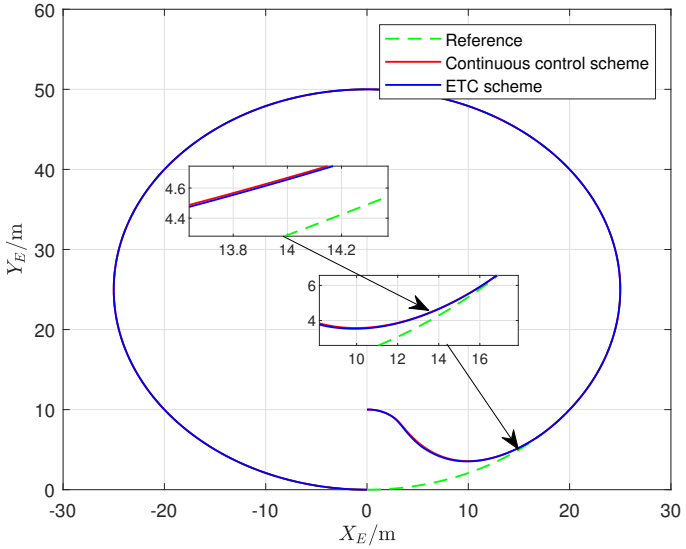

Figure 1. Actual and reference trajectories in (x, y) plane.

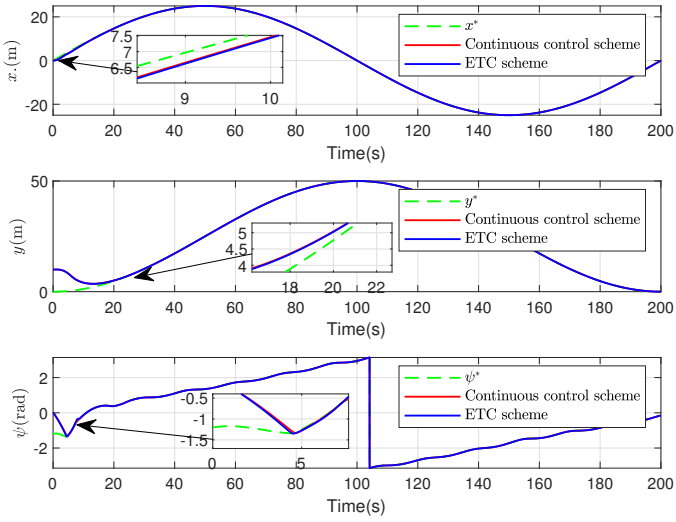

Figure 2. Time evolution of actual position and heading angle.

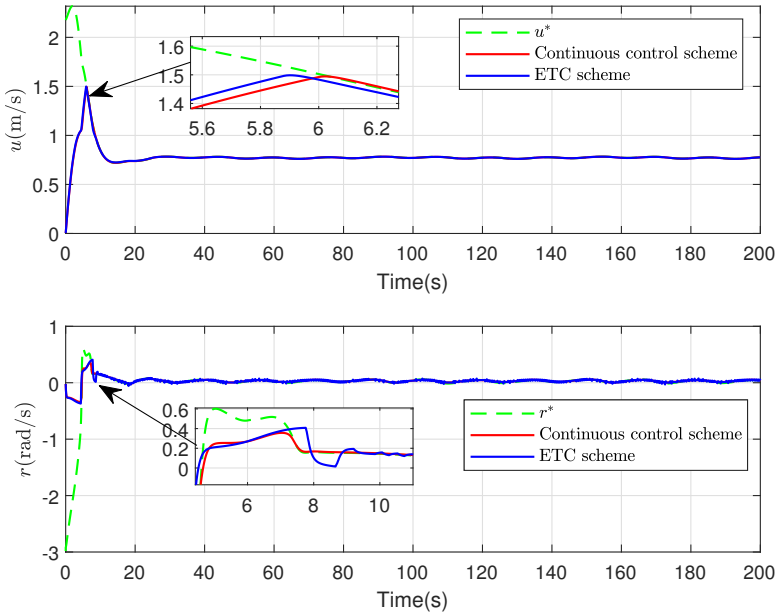

Figure 3. Surge velocity and yaw rate.

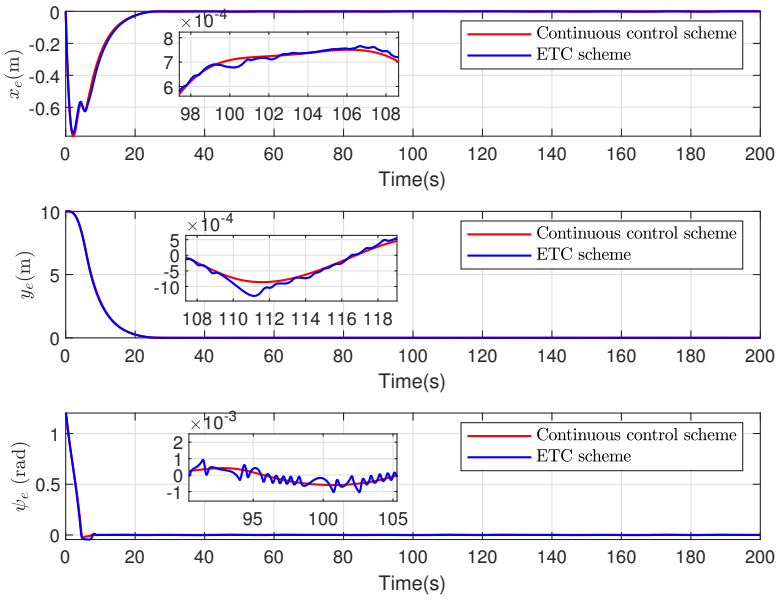

Figure 4. Time evolution of the trajectory tracking errors.

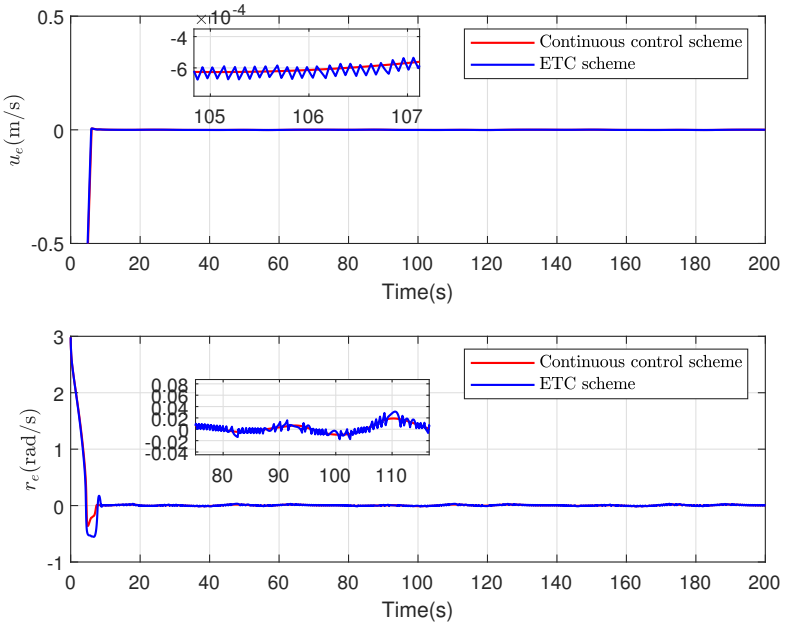

Figure 5. Time evolution of the velocity errors.

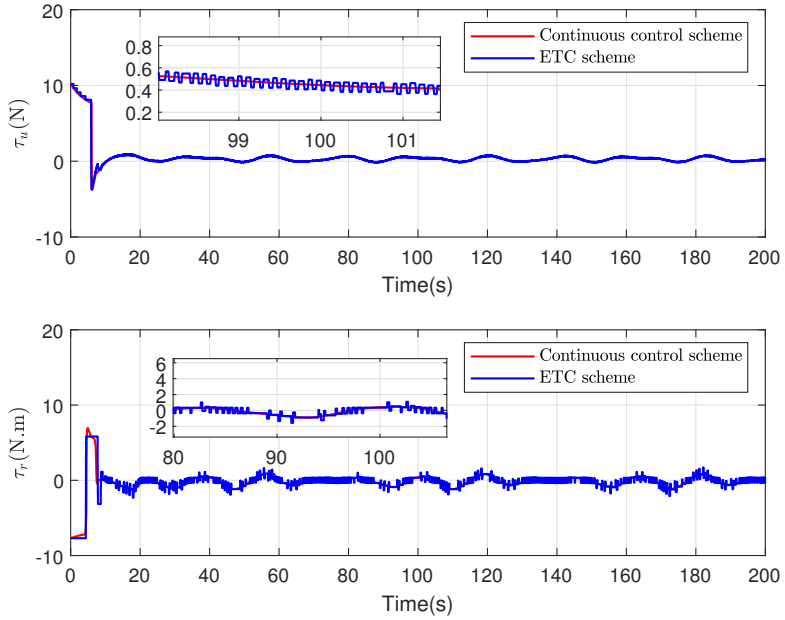

Figure 6. Time evolution of the control input.

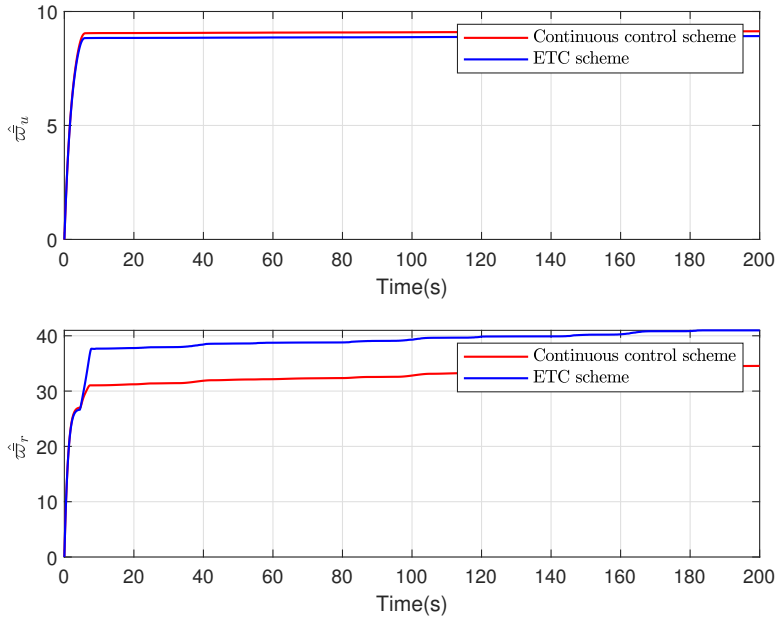

Figure 7. Curve of estimation $\hat{\bar{\omega}}_u$ and $\hat{\bar{\omega}}_u$.

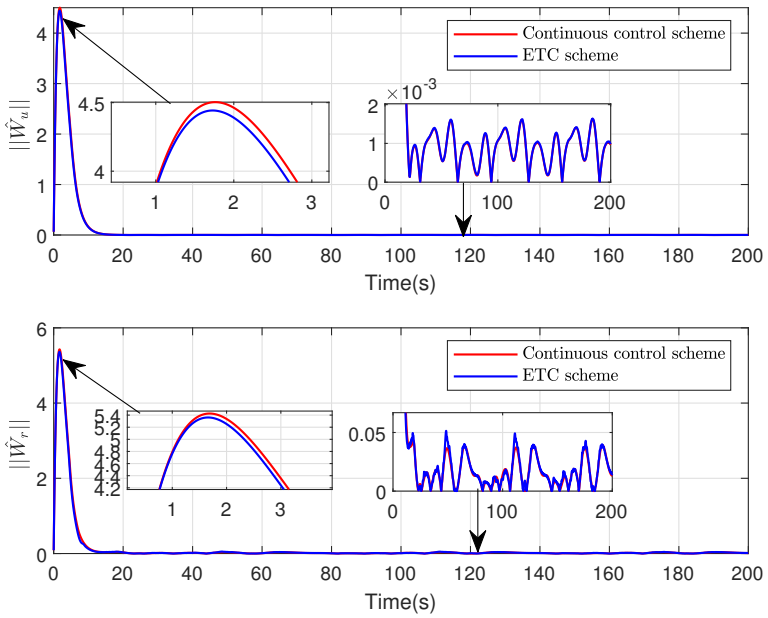

Figure 8. Curve of estimation $\hat{W}_u$ and $\hat{W}_r$.

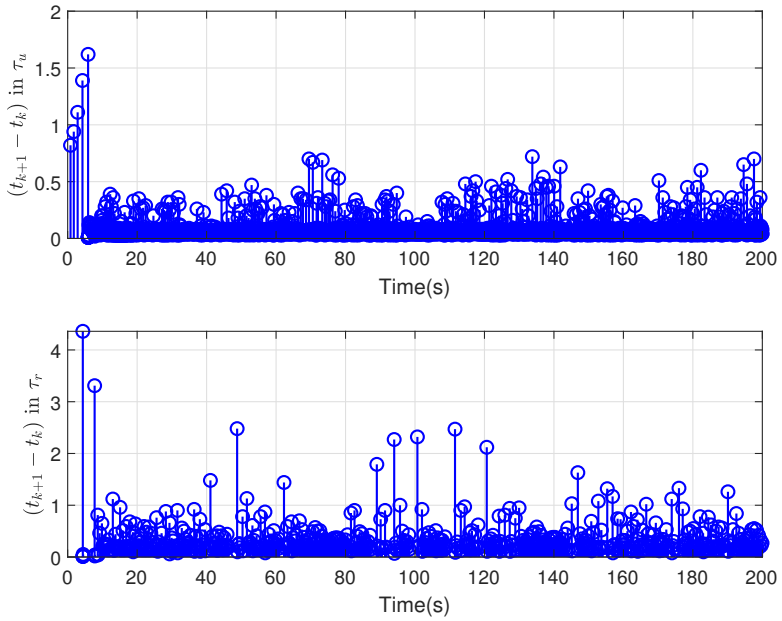

Figure 9. Time evolution of the interevent time.

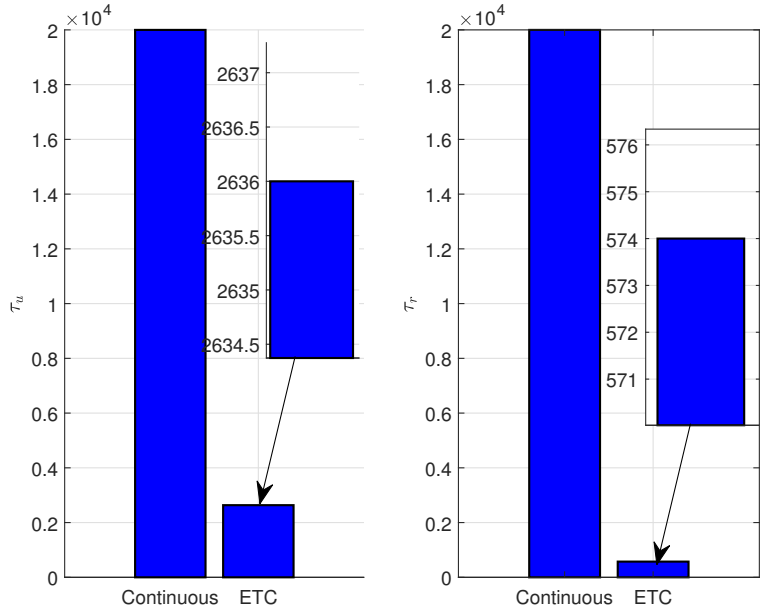

Figure 10. The number of controller updates.

4.2. Simulation experiment 2

The trapezoidal reference trajectory is as follows

$$\begin{cases} y^* = 10 & t \le 47 \\ y^* = \sqrt{100-(t-47)^2} & 47 < t \le 53 \\ y^* = \frac{65-t}{1.5} & 53 < t \le 62 \\ y^* = 10 - \sqrt{100-(t-68)^2} & 62 < t \le 68 \\ y^* = 0 & 68 < t \le 112 \\ y^* = 10 - \sqrt{100-(t-112)^2} & 112 < t \le 118 \\ y^* = \frac{t-115}{1.5} & 118 < t \le 127 \\ y^* = \sqrt{100-(t-133)^2} & 127 < t \le 133 \\ y^* = 10 & 133 < t \le 200 \end{cases} \tag{4.6}$$

The controller parameters under the trapezoidal reference trajectory are shown in Table 3.

Table 3. Controller parameters.

Trapezoidal trajectory	$k_{11} = 0.2$	$k_{12} = 0.05$	$k_{21} = 1.5$	$k_{22} = 0.2$
	$k_{31} = 1.9$	$k_{32} = 0.7$	$k_{41} = 1.5$	$k_{42} = 1.5$
	c_1=1	$\iota_1 = 1$	$c_2 = 0.001$	$\iota_1 = 3$
	$\varsigma_z = 0.05$	$\varsigma_\psi = 0.05$	$\varsigma_u = 0.05$	$\varsigma_r = 0.05$
	$\eta_{11} = 0.05$	$\eta_{12} = 0.05$	$\eta_{21} = 0.05$	$\eta_{22} = 0.05$
	$\varepsilon_u = 0.05$	$\varepsilon_r = 0.05$		

Table 4. Performance index comparison of the schemes of ETC and FTC.

		ETC scheme	FTC scheme
IAE	$x - x^*$	8.8848	9.2154
	$y - y^*$	17.4747	17.5333
MIAC	τ_u	1.4084	1.0757
	τ_r	1.4065	0.8849

The simulation results under the trapezoidal trajectory are shown in Figures 11–20 and Table 4. Under the trapezoidal trajectory, the two fault-tolerant control schemes also show excellent tracking performance. Figures 14 and 15 show that the tracking error and velocity error of the system are within a small range. According to the performance indicators given by IAE in Table 4, we find that the tracking performance of the ETC control scheme is slightly better than that of the FTC control scheme. Figure 20 shows that under the FTC control scheme, the update of the controller are also 20,000 times, while the FTC are 4795 and 612 times. Furthermore, according to the performance index data in Table 4, the energy consumption of the ETC scheme is slightly higher than that of the FTC scheme. Figures 17 and 18 show that the estimates of NNs weights and uncertainty terms are bounded. The above data show that all signals in the closed-loop tracking system are bounded, and the proposed ETC control scheme effectively solves the problems of actuator failure, input saturation, and communication resource limitation.

In addition, the ETC scheme in this paper is essentially an active fault-tolerant control method, while the even FTC scheme is actually a passive fault-tolerant control method. FTC can improve the

steady state of the system, and ETC can reduce the operating frequency of the controller. In the actual system, the introduction of ETC will inevitably sacrifice part of the control performance. However, the method of compensating fault factors by event-triggered mechanism in this paper finally obtains the control effect almost indistinguishable from the continuous FTC scheme, and effectively reduces the frequency of controller update and the frequency of actuator wear.

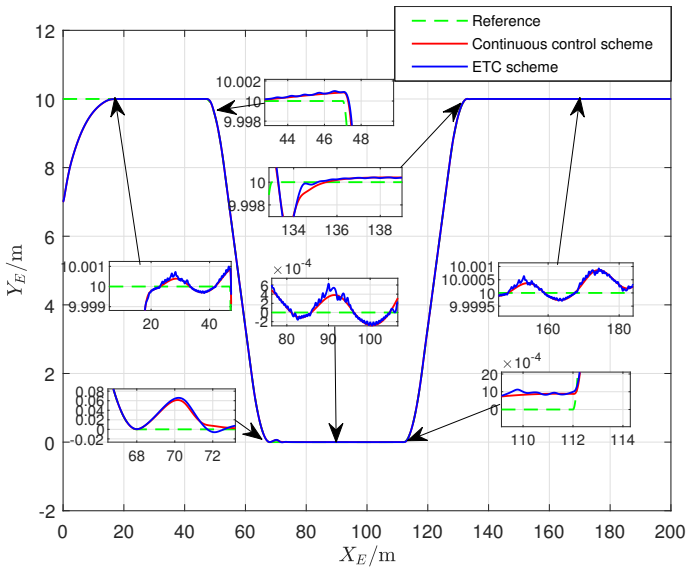

Figure 11. Actual and reference trajectories in (x, y) plane.

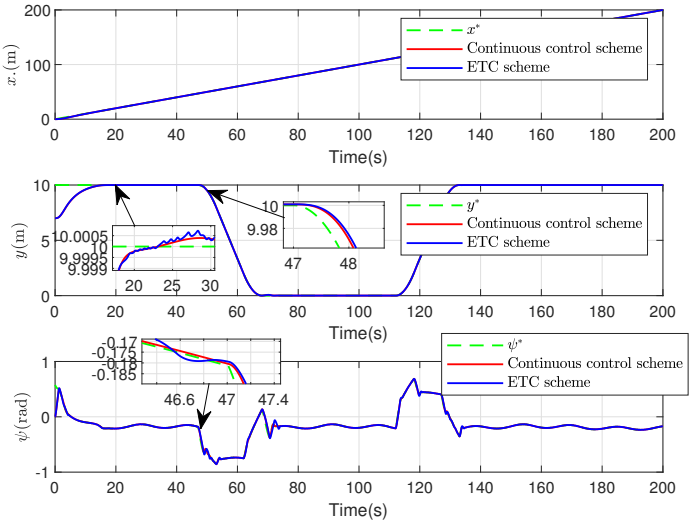

Figure 12. Time evolution of actual position and heading angle.

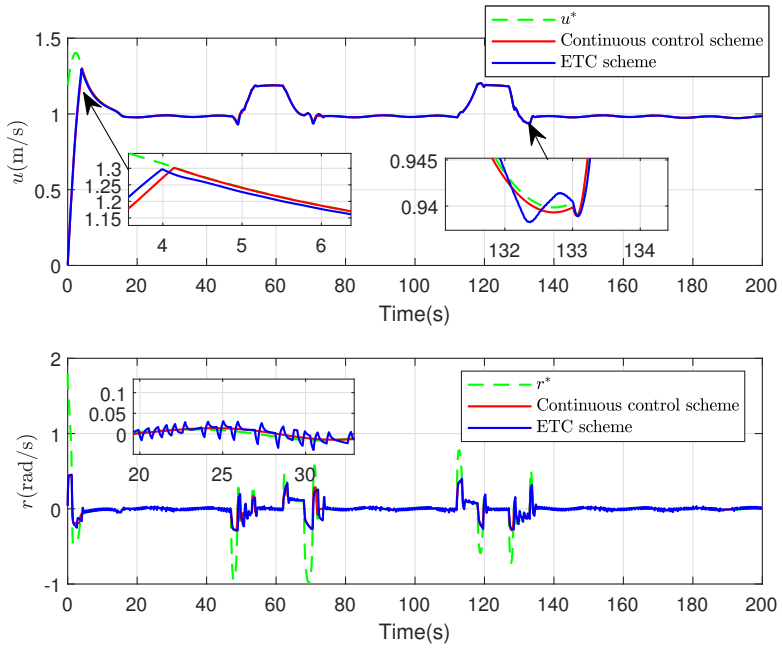

Figure 13. Surge velocity and yaw rate.

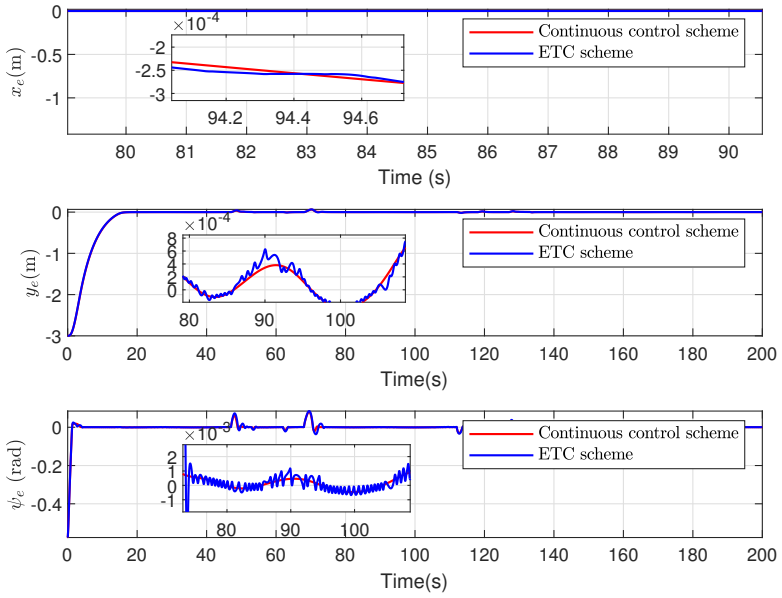

Figure 14. Time evolution of the trajectory tracking errors.

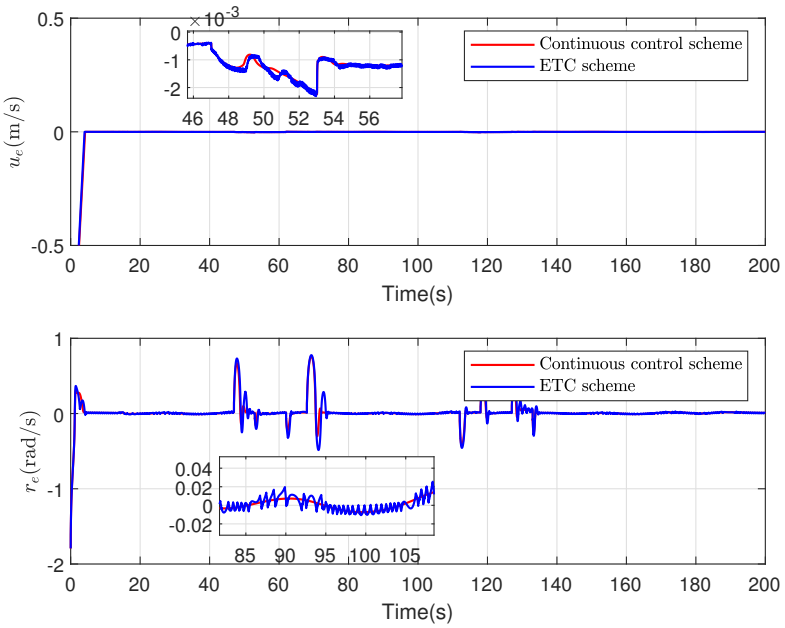

Figure 15. Time evolution of the velocity errors.

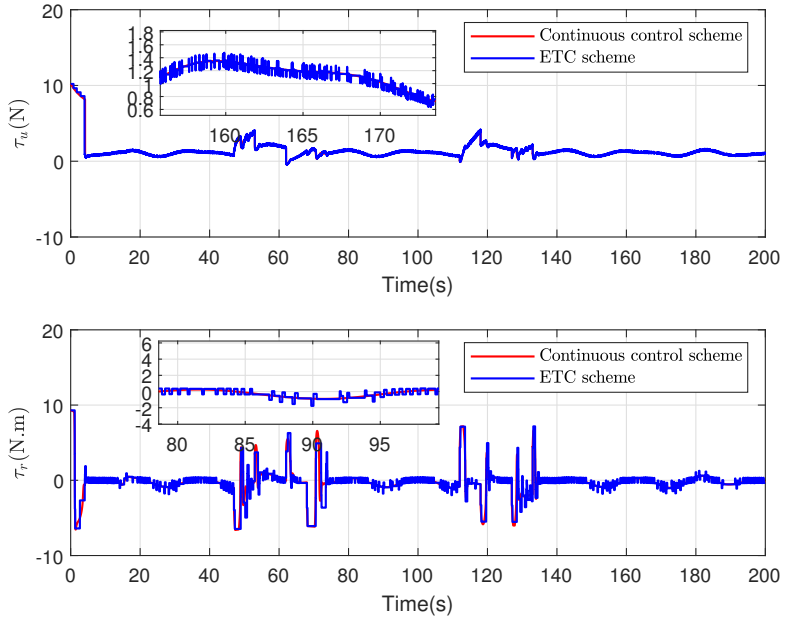

Figure 16. Time evolution of the control input.

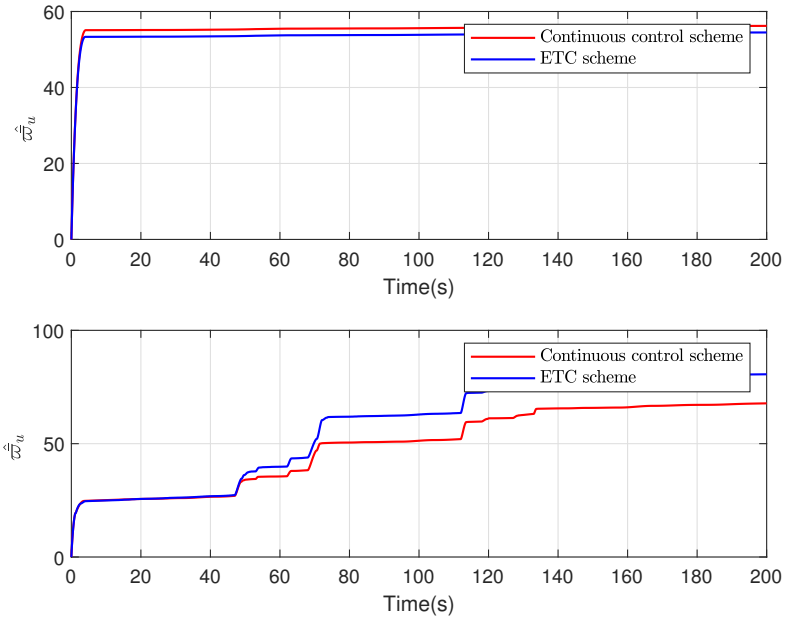

Figure 17. Curve of estimation $\hat{\bar{\omega}}_u$ and $\hat{\bar{\omega}}_u$.

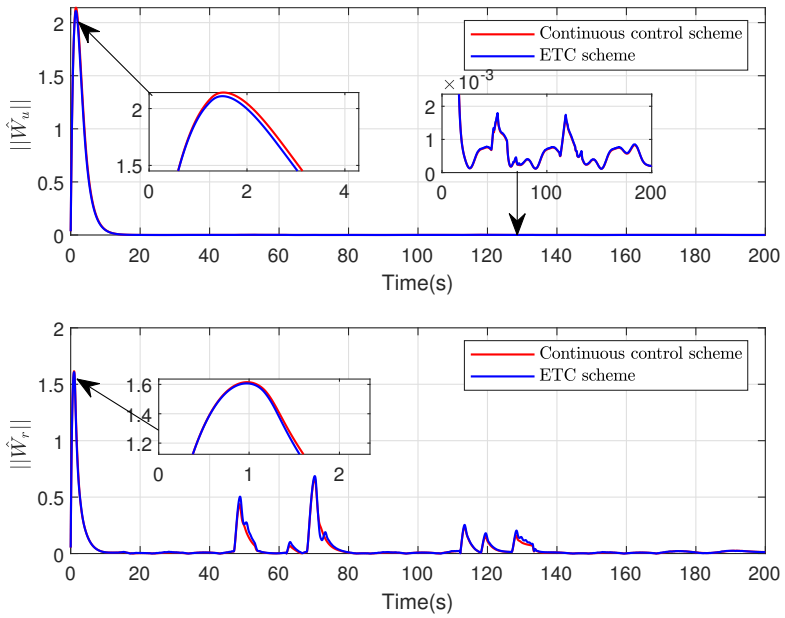

Figure 18. Curve of estimation $\hat{W}_u$ and $\hat{W}_r$.

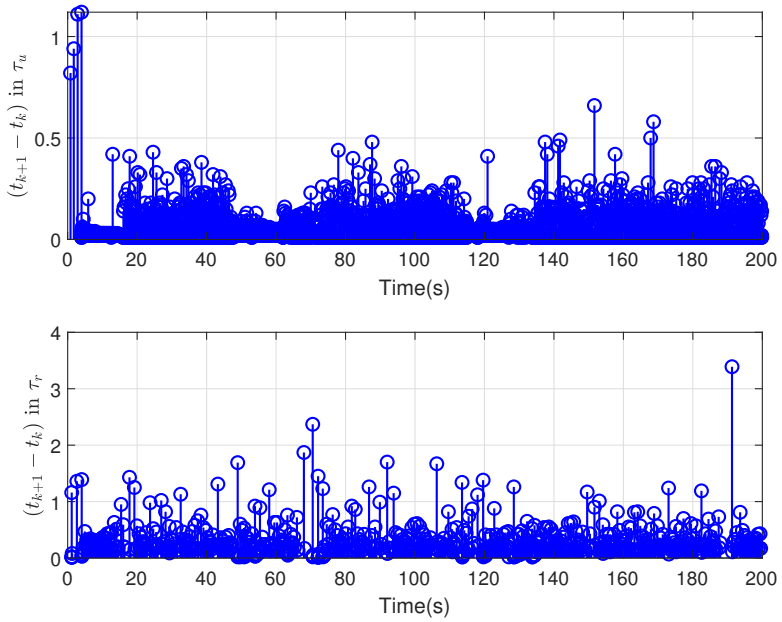

Figure 19. Time evolution of the interevent time.

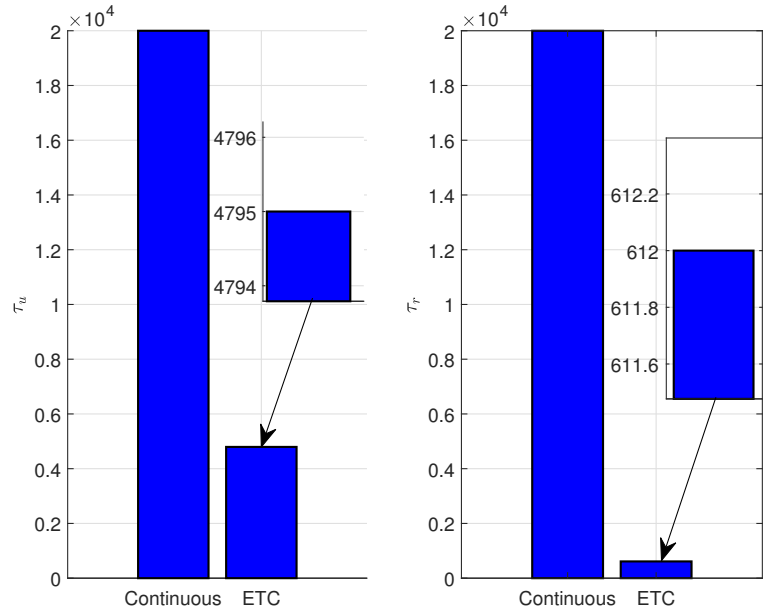

Figure 20. The number of controller updates.

In summary, through the verification and analysis of two sets of simulation experiments, the ETC control scheme designed in this paper has demonstrated several superior performances in solving actuator faults, dealing with external interference, reducing the frequency of control commands and ensuring

high-precision tracking effects. Moreover, the controller designed in this paper has a concise structure and is easier to apply in engineering.

5. Conclusions

In this paper, a novel fault-tolerant control scheme is designed for USVs. By introducing MLPs technology, the uncertain dynamics, unknown interference, and fault factors of the system are converted into the form of single parameter. Since the controller involves only the adjustment of a single parameter, the structure of the controller in this paper is simple and easy to apply in practice. Upon non-respect of the response of the event-triggered mechanism, the communication resources occupied by the control scheme presented in this paper will be lower in the actual system. The theoretical analysis shows that the ETC control scheme designed in this paper ensures that all the error signals of the USVs system converge to a small set around the origin in a finite time, and all the signals in the tracking system are bounded.

Acknowledgments

The authors would like to acknowledge the National Natural Science Foundation of China (NSFC51779136), Science and Technology Commission of Shanghai Municipality (NO.20dz1206002).

Conflict of interest

The authors declare there are no conflict of interest.

References

1. W. Wu, Z. Peng, D. Wang, L. Liu, Q. L. Han, Network-based line-of-sight path tracking of underactuated unmanned surface vehicles with experiment results, *IEEE Trans. Cybern.*, **52** (2021), 10937–10947. https://doi.org/10.1109/TCYB.2021.3074396
2. Y. Zhao, X. Qi, Y. Ma, Z. Li, R. Malekian, M. A. Sotelo, Path following optimization for an underactuated usv using smoothly-convergent deep reinforcement learning, *IEEE Trans. Intell. Transp. Syst.*, **22** (2021), 6208–6220. https://doi.org/10.1109/TITS.2020.2989352
3. N. Wang, Y. Gao, H. Zhao, C. K. Ahn, Reinforcement learning-based optimal tracking control of an unknown unmanned surface vehicle, *IEEE Trans. Neural Networks Learn. Syst.*, **32** (2020), 3034–3045. https://doi.org/10.1109/TNNLS.2020.3009214
4. M. Liu, F. Zhao, J. L. Yin, J. W. Niu, Y. Liu, Reinforcement-tracking: an effective trajectory tracking and navigation method for autonomous urban driving, *IEEE Trans. Intell. Transp. Syst.*, **23** (2021), 6991–7007. https://doi.org/10.1109/TITS.2021.3066366
5. Z. P. Yan, H. Y. Yang, W. Zhang, F. T. Lin, Q. S. Gong, Y. Zhang, Bionic fish tail design and trajectory tracking control, *Ocean Eng.*, **257** (2022), 111659. https://doi.org/10.1016/j.oceaneng.2022.111659

6. X. X. Liu, W. Wang, X. L. Li, F. S. Liu, Z. H. He, Y. Z. Yao, et al., MPC-based high-speed trajectory tracking for 4WIS robot, *ISA Trans.*, **123** (2022), 413–424. https://doi.org/10.1016/j.isatra.2021.05.018
7. K. Y. Pettersen, F. Mazenc, H. Nijmeijer, Global uniform asymptotic stabilization of an underactuated surface vessel: Experimental results, *IEEE Trans. Control Syst. Technol.*, **12** (2004), 891–903. https://doi.org/10.1109/TCST.2004.833643
8. K. D. Do, Practical control of underactuated ships, *Ocean Eng.*, **37** (2010), 1111–1119. https://doi.org/10.1016/j.oceaneng.2010.04.007
9. G. Q. Zhang, J. Q. Li, X. Jin, C. Liu, Robust adaptive neural control for wing-sail-assisted vehicle via the multiport event-triggered approach, *IEEE Trans. Cybern.*, **2021** (2021). https://doi.org/10.1109/TCYB.2021.3091580
10. G. B. Zhu, M. Yong, S. L. Hu, Single-parameter-learning-based finite-time tracking control of underactuated MSVs under input saturation, *Control Eng. Pract.*, **105** (2020), 104652. https://doi.org/10.1016/j.conengprac.2020.104652
11. G. B. Zhu, J. L. Du, Global robust adaptive trajectory tracking control for surface ships under input saturation, *IEEE J. Ocean. Eng.*, **45** (2020), 442–450. https://doi.org/10.1109/JOE.2018.2877895
12. Z. W. Zheng, Y. T. Huang, L. H. Xie, B. Zhu, Adaptive trajectory tracking control of a fully actuated surface vessel with asymmetrically constrained input and output, *IEEE Trans. Control Syst. Technol.*, **26** (2018), 1851–1859. https://doi.org/10.1109/TCST.2017.2728518
13. B. Zhou, B. Huang, Y. M. Su, Y. X. Zheng, S. Zheng, Fixed-time neural network trajectory tracking control for underactuated surface vessels, *Ocean Eng.*, **236** (2021), 109416. https://doi.org/10.1016/j.oceaneng.2021.109416
14. L. H. Kong, W. He, C. G. Yang, G. Li, Z. Q. Zhang, Adaptive fuzzy control for a marine vessel with time-varying constraints, *IET Control Theory Appl.*, **12** (2018), 1448–1455. https://doi.org/10.1049/iet-cta.2017.0757
15. C. F. Huang, X. K. Zhang, G. Q. Zhang, Improved decentralized finite-time formation control of underactuated USVs via a novel disturbance observer, *Ocean Eng.*, **174** (2019), 117–124. https://doi.org/10.1016/j.oceaneng.2019.01.043
16. Q. Zhang, G. B. Zhu, X Hu, R. M. Yang, Adaptive neural network auto-berthing control of marine ships, *Ocean Eng.*, **17** (2019), 40–48. https://doi.org/10.1016/j.oceaneng.2019.02.031
17. Y. Ma, G. B. Zhu, Z. X. Li, Error-driven-based nonlinear feedback recursive design for adaptive NN trajectory tracking control of surface ships with input saturation, *IEEE Intell. Transp. Syst. Mag.*, **11** (2019), 17–28. https://doi.org/10.1109/MITS.2019.2903517
18. J. P. Cai, C. Y. Wen, H. Y. Su, Z. T. Liu, Robust adaptive failure compensation of hysteretic actuators for a class of uncertain nonlinear systems, *IEEE Trans. Autom. Control.*, **58** (2013), 2388–2394. https://doi.org/10.1109/TAC.2013.2251795
19. X. D. Tang, G. Tao, S. M. Joshi, Adaptive output feedback actuator failure compensation for a class of non-linear systems, *Int. J. Adapt. Control Signal Process.*, **19** (2005), 419–444. https://doi.org/10.1002/acs.843

20. Y. L. Wang, Q. L. Han, Network-based fault detection filter and controller coordinated design for unmanned surface vehicles in network environments, *IEEE Trans. Ind. Inf.*, **12** (2016), 1753–1765. https://doi.org/10.1109/TII.2016.2526648

21. Z. W. Zheng, L. Sun, L. H. Xie, Error-constrained LOS path following of a surface vessel with actuator saturation and faults, *IEEE Trans. Syst. Man. Cybern Syst.*, **48** (2018), 1794–1805. https://doi.org/10.1109/TSMC.2017.2717850

22. Y. J. Deng, X. K. Zhang, N. Im, G. Q. Zhang, Q. Zhang, Model-based event-triggered tracking control of underactuated surface vessels with minimum learning parameters, *IEEE Trans. Neural Networks Learn. Syst.*, **31** (2020), 4001–4014. https://doi.org/10.1109/TNNLS.2019.2951709

23. S. L. Yu, J. S. Lu, G. B. Zhu, S. J. Yang, Event-triggered finite-time tracking control of underactuated MSVs based on neural network disturbance observer, *Ocean Eng.*, **253** (2022), 111169. https://doi.org/10.1016/j.oceaneng.2022.111169

24. Y. J. Deng, X. K. Zhang, Event-triggered composite adaptive fuzzy output-feedback control for path following of autonomous surface vessels, *IEEE Trans. Fuzzy Syst.*, **29** (2021), 2701–2713. https://doi.org/10.1109/TFUZZ.2020.3006562

25. L. T. Xing, C. Y. Wen, Z. T. Liu, H. Y. Su, J. P. Cai, Adaptive compensation for actuator failures with event-triggered input, *Automatica*, **85** (2017), 129–136. https://doi.org/10.1016/j.automatica.2017.07.061

26. G. Q. Zhang, S. Gao, J. Q. Li, W. D. Zhang, Adaptive neural fault-tolerant control for course tracking of unmanned surface vehicle with event-triggered input, *Proc. Inst. Mech. Eng., Part I: J. Syst. Control Eng.*, **235** (2021), 1594–1604. https://doi.org/10.1177/09596518211013155

27. G. B. Zhu, Y. Ma. Z. X. Li, R. Malekian, M. Sotelo, Event-triggered adaptive neural fault-tolerant control of underactuated MSVs with input saturation, *IEEE Trans. Intell. Transp. Syst.*, **23** (2021), 7045–7057. https://doi.org/10.1109/TITS.2021.3066461

28. Y. P. Weng, N. Wang, Finite-time observer-based model-free time-varying sliding-mode control of disturbed surface vessels, *Ocean Eng.*, **251** (2022), 110866.https://doi.org/10.1016/j.oceaneng.2022.110866

29. N. Wang, Y. Gao, C. Yang, X. F. Zhang, Reinforcement learning-based finite-time tracking control of an unknown unmanned surface vehicle with input constraints, *Neurocomputing*, **484** (2022), 26–37. https://doi.org/10.1016/j.neucom.2021.04.133

30. Y. L. Yu, C. Guo, T. S. Li, Finite-time los path following of unmanned surface vessels with time-varying sideslip angles and input saturation, *IEEE/ASME Trans. Mechatron.*, **27** (2022), 463–474. https://doi.org/10.1109/TMECH.2021.3066211

31. N. Wang, H. K. He, Dynamics-level finite-time fuzzy monocular visual servo of an unmanned surface vehicle, *IEEE Trans. Ind. Electron.*, **67** (2020), 9648–9658. https://doi.org/10.1109/TIE.2019.2952786

32. M. Y. Fu, L. L. Wang, Finite-time coordinated path following control of underactuated surface vehicles based on event-triggered mechanism, *Ocean Eng.*, **246** (2022), 110530.https://10.1016/j.oceaneng.2022.110530

33. T. I. Fossen, *Handbook of Marine Craft Hydrodynamics and Motion Control*, John Wiley & Sons, New York, NY, USA, 2011.
34. F. Wang, B. Chen, X. P. Liu, C. Lin. Finite-time adaptive fuzzy tracking control design for nonlinear systems, *IEEE Trans. Fuzzy Syst.*, **26** (2018), 1207–1216. https://doi.org/10.1109/TFUZZ.2017.2717804
35. Z. W. Zheng, M. Feroskhan, L. Sun, Adaptive fixed-time trajectory tracking control of a stratospheric airship, *ISA Trans.*, **76** (2018), 134–144. https://doi.org/10.1016/j.isatra.2018.03.016
36. S. H. Yu, X. H. Yu, B. Shirinzadeh, Z. H. Man, Continuous finite-time control for robotic manipulators with terminal sliding mode, *Automatica*, **41** (2005), 1957–1964. https://doi.org/10.1016/j.automatica.2005.07.001
37. R. M. Sanner, J. J. E. Slotine, Gaussian networks for direct adaptive control, *IEEE Trans. Neural Network Learn. Syst.*, **3** (1992), 837–863. https://doi.org/10.1109/72.165588
38. A. J. Kurdila, F. J. Narcowich, J. D. Ward, Persistency of excitation in identification using radial basis function approximants, *SIAM J. Control Optim.*, **33** (1995), 625–642. https://doi.org/10.1137/S0363012992232555
39. C. L. Wang, Y. Lin, Decentralized adaptive tracking control for a class of interconnected nonlinear time-varying systems, *Automatica*, **54** (2015), 16–24. https://doi.org/10.1016/j.automatica.2015.01.041
40. M. M. Polycarpon, Stable adaptive neural control scheme for nonlinear systems, *IEEE Trans. Autom. Control*, **41** (1996), 447–451. https://doi.org/10.1109/9.486648
41. B. S. Park, J. W. Kwon, H. Kim, Neural network-based output feedback control for reference tracking of underactuated surface vessels, *Automatica*, **77** (2017), 353–359. https://doi.org/10.1016/j.automatica.2016.11.024

AIMS Press